*Clays and Clay Minerals*, Vol. 52, No. 6, 779–791, 2004.

# Fe-RICH CLAYS IN A WEATHERING PROFILE DEVELOPED FROM SERPENTINITE

J. CAILLAUD[1,*], D. PROUST[1], D. RIGHI[1] AND F. MARTIN[2]

[1] UMR 6532 CNRS, HydrASA, Faculté des Sciences, 40 av. du recteur Pineau, 86022 Poitiers cedex, France
[2] UMR 6532 CNRS, HydrASA, Facultés des Sciences, 123, av. A. Thomas, 87060 Limoges cedex, France

**Abstract**—Bulk mineralogical and chemical properties of a weathering profile derived from serpentinite were studied using classical pedological methods (Munsell soil colors, particle-size distribution, density, cation exchange capacity, exchangeable bases, among others) and inductively coupled plasma-atomic emission spectroscopy (ICP-AES) results. Bulk clay fractions were characterized using X-ray diffraction, thermal analysis, electron microprobe, Mössbauer and infrared spectroscopies. Bulk geochemical mass-balance calculated from ICP-AES results shows leaching of both Mg and Si which reflects the early weathering of serpentine minerals. As a consequence, newly formed clay minerals are enriched with the least mobile elements, *i.e.* Fe and Al, producing dioctahedral smectites. These dioctahedral smectites are complex, heterogeneous and consist mainly of two populations. One population is an Fe-rich montmorillonite with little or no tetrahedral charge and $Fe^{3+}$ as the dominant octahedral cation whereas the second population exhibits tetrahedral charge. Both populations occur as interstratified layers in the lower horizon of the weathering profile but show increasing segregation into well-defined end-members towards the surface horizons. Considering total Al and Fe contents, these clays differentiate into two chemical composition domains, Fe-rich clays in the lower profile and Al-rich clays towards the surface horizons.

**Key Words**—Serpentinite, Smectite, Soil, Ultrabasic Rock, Weathering.

## INTRODUCTION

Ultrabasic-rock weathering under tropical conditions has been studied widely over the last three decades because of the great economic interest in ore deposits (Trescases, 1969, 1975, 1986; Besset, 1978; Golighty, 1981; Pelletier, 1983; Gaudin, 2002). It is also widely recognized that serpentine-derived soils are quite different from those developed on other parent materials. Studies deal with mineralogical and chemical properties of serpentinite-derived pedons and their relationships with vegetation (Rabenhorts *et al*., 1982; Alexander *et al*., 1989; Graham *et al*., 1990; Bulmer and Lavkulich, 1994). Alexander (1988) showed that landscapes developed from unserpentinized ultramafic rocks such as peridotite were more stable than landscapes developed from serpentinized rocks. Cleaves *et al*. (1974) compared the contrasting weathering processes of two mineralogically and chemically distinct rock types, a serpentinite and a schist, in the same climatic (temperate climate) and topographic conditions. The serpentinite soils contained relatively small amounts of quartz, chalcedony and 14 Å clay minerals, whereas schist soils contained large amounts of clay minerals and gibbsite. The absence of saprolite in the serpentinite profile was attributed to the lack of weathering-resistant minerals. Pedological studies showed that two types of soil can develop from the serpentinite, *i.e.* a well drained soil with a very thin (mm) C horizon (saprock) and a thick, poorly drained soil, with well developed (m) saprock and saprolite (Coombe *et al*., 1956; Isok and Harward, 1982; Bonifacio *et al*., 1996). Berre *et al*. (1974) showed that these two types of soils occurred on a small serpentinite body of La Roche l'Abeille (Massif Central, France) with dioctahedral beidellite-type smectite as the dominant clay mineral in the thickest, poorly drained soil type. Ducloux *et al*. (1976) showed that whole soils on this serpentinite body contain nontronitic smectite, some soil chlorites and locally, mixed-layer chlorite-vermiculite. Isok and Harward (1982) found only serpentine and chlorite in well-drained soil whereas they identified some smectite in the thickest soil in addition to the serpentine and chlorite. Bonifacio *et al*. (1996) observed that vermiculite was present in upper and drier horizons whereas low-charged smectite occurred in poorly drained conditions. Wildman *et al*. (1968) identified Fe-rich montmorillonite as the dominant clay mineral in the B horizons of serpentinite-derived soils.

These studies demonstrate the large variety of clay phases produced by serpentine weathering processes and the influence of topographic position upon the development of the weathering profiles. The aim of this work was thus to improve our knowledge about the weathering processes of serpentinite under an oceanic temperate climate and their influence upon the crystallochemistry of newly formed clay minerals. As a consequence, this study was focused on a thick poorly-drained soil developed at the summit of a serpentinite body in order to follow clay mineral crystallization through a

* E-mail address of corresponding author:
jacinthe.caillaud@hydrasa.univ-poitiers.fr
DOI: 10.1346/CCMN.2004.05206013

complete weathering profile including saprock and saprolite horizons.

## MATERIALS AND METHODS

### *Materials*

The samples were collected from a weathering profile developed on a serpentinite body (Saint-Laurent moor) located 30 km south of Limoges near La Roche l'Abeille (Limousin, France). The profile is located at the summit of the hill (360–380 m altitude) with a slight dip ranging from 20º to 25º North. The joints are abundant and mainly oriented N 23º East and N 28º West (N'Kanika, 1979).

The unweathered rock observed at the bottom of the profile is serpentinite containing serpentine (70–85%), magnesian chlorite (10–15%) and magnetite. The profile (Figure 1) is ~140 cm thick and shows, from bottom to top, three alteration zones: (1) unweathered rock; (2) the saprock where coherent rock structure is still preserved and primary minerals are still interconnected; (3) the saprolite in which the texture of the original rock is destroyed and replaced by a mixture of clay associated with oxyhydroxides and relics of primary minerals. This zone shows a prismatic structure generated by wetting and drying cycles in the deeply argillized rock; the structure grades into polyhedric towards the surface. In addition, an allochthonous deposit covers the weathering profile. It contains feldspars and quartz resulting from erosion of the Massif Central. No chlorite was detected in X-ray diffraction (XRD) patterns of the allochthonous deposit, whereas some tremolite derived from a northern amphibolite facies was noticed. This reworked horizon and its related soil were not studied in this work.

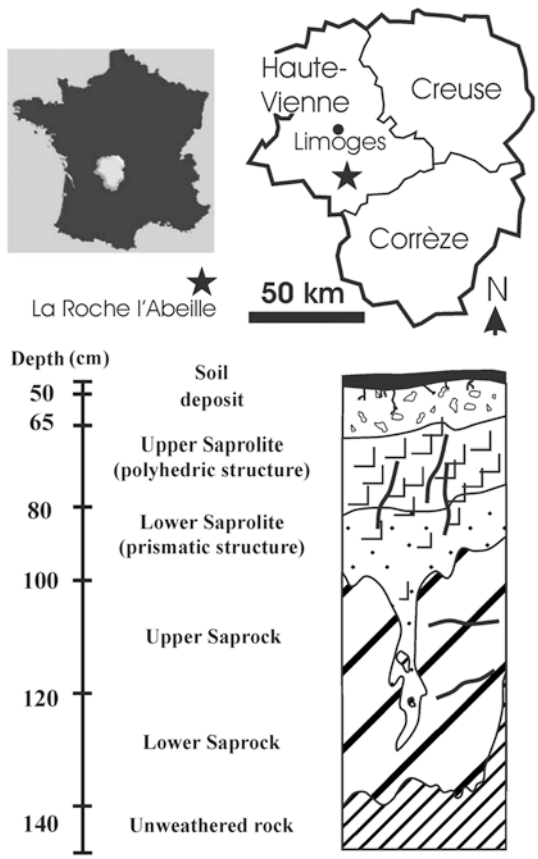


Figure 1. Location and sketch of the serpentinite weathering profile.

### *Methods*

Samples were collected from the unweathered rock, the saprock and the saprolite (1) to make thin-sections for petrographic analyses, (2) to study soil properties of bulk, or <2 mm sized fractions, and (3) to characterize the bulk clay fraction in each weathering zone.

The petrographic data were recorded from thin-sections studied by optical microscopy under natural and polarized light (Olympus BH2). In order to establish a geochemical mass-balance, apparent densities were obtained from undisturbed paraffin-coated samples by the difference between weight measured in air and in water. Bulk chemical analyses were achieved by ICP-AES (CRPG Nancy), using a JOBIN-YVON JY 70 spectrometer on total powders after fusing with LiBr and dissolution in 1 N HCl.

Geochemical changes between rock and weathered samples were calculated using two procedures: (1) the oxide concentration of each element was transformed using the log function in order to display on the same scale small and the large oxide amounts. The relative element variation between concentrations for a weathered sample ($C_B$) and the rock sample ($C_A$) was obtained using equation 1:

$$\text{Element relative variation} = \log (C_B/C_A) = \log (C_B) - \log (C_A)$$

(2) A more detailed bulk geochemical balance including volume and/or mass differences due to weathering processes was calculated using Gresens (1967) equation:

$$X_i = a\,[f_v\,(g_B/g_A)\,C_i^B - C_i^A] \qquad (2)$$

where $X_i$, is the amount of element i gained or lost (in g), $f_v$ is the volume factor (ratio between the weathered sample ($V_B$) and the rock ($V_A$) volumes), $g_A$ and $g_B$ are apparent densities of rock (A) and weathered sample (B), $C_i^A$ and $C_i^B$ are the concentrations of component i in rock A and weathered sample B (g/100 g), $a$ is the reference mass of the original sample ($a$ = 100 g because chemical analyses were normalized to 100 g).

If $f_v = 1$, isovolumetric weathering occurs, whereas $f_v < 1$ or $f_v > 1$ denotes volume loss or gain respectively.

Composition-volume diagrams derived from equation 2 can be used to assess element mass transfer during

https://doi.org/10.1346/CCMN.2004.05206013 Published online by Cambridge University Press

weathering assuming, either (1) isovolumetric conditions, or (2) immobility of one element chosen as reference.

(1) The first case means that $f_V = 1$. This condition may be applied to the saprock horizons where the rock structure is well preserved. In composition-volume diagrams, the vertical line at $f_V = 1$ on the X coordinate intersects the other oxide lines. The value on the Y coordinate is the gain (positive value) or loss (negative value) of oxides during the weathering.

(2) The second case is more convenient for saprolite horizons where the structure is destroyed ($f_V \neq 1$). Aluminum was chosen as the reference element considering that (a) in the range of the pH values (6.80–7.00) measured in the bulk samples (see Table 3) Al is immobile (Reesman *et al*., 1969; Wesolowski, 1992), (b) chlorite which is the only Al-bearing mineral in the rock, remains only slightly weathered throughout the profile. Moreover, (c) even when some Al is leached during mineral-weathering processes, it migrates only a short distance before being trapped in the secondary minerals. The overall result, at the scale of the bulk sample, is that Al content does not change and that this element can be considered as the immobile reference. This condition implies that $X\ Al_2O_3 = 0$. In composition-volume diagrams, the vertical line at the $f_v$ value corresponding to $X\ Al_2O_3 = 0$ on the X coordinate intersects the other oxide. The value on the Y coordinate is the gain (positive value) or loss (negative value) of oxides during the weathering, assuming immobile Al.

Various forms of Fe, Al and Si were extracted using 2 g of total sample from each horizon, and the solutions were analyzed using ICP-AES. The amounts extracted were compared to their total amounts obtained from ICP-AES analyses of the bulk sample powders. Dithionite-soluble Fe ($Fe_d$), Al ($Al_d$) and Si ($Si_d$) corresponding to the poorly ordered inorganic and organic, and crystalline components (Smith and Mitchell, 1987), respectively, were determined according to the method of Mehra and Jackson (1960), and oxalate-extractable Fe ($Fe_o$), Al ($Al_o$) and Si ($Si_o$), corresponding to the poorly ordered inorganic and organic components, respectively, (Smith and Mitchell, 1987), by the method of Schwertmann (1964).

The magnetic particles were separated from the total powder with a hand magnet and identified by XRD.

The soil properties (organic carbon content, pH, particle-size distribution, and cation exchange capacity (CEC)) were studied on the <2 mm size fraction. The pH was measured in water. The CEC was obtained using 1 M ammonium acetate at pH 7, and ammonium exchangeable cations were measured by ICP-AES. Particle-size analysis was performed after destruction of organic matter with $H_2O_2$ using sedimentation methods.

Clay fractions were extracted using continuous-flow centrifugation (Beckman J2-21 equipped with the JCF-Z continuous flow rotor), separated into four granulometric fractions: <0.05 μm, 0.05–0.2 μm, 0.2–1 μm, 1–2 μm and saturated with Ca.

Pressed pellets from the <0.05 μm clay fraction were analyzed using a CAMECA SX 50 electron microprobe (Service CAMPARIS, Université ParisVI) with wavelength-dispersive spectrometers (WDS). The major elements analyzed were Na, Mg, Al, Si, K, Ca, Ti, Mn and Fe. The microprobe was calibrated using synthetic and natural oxides. Corrections were made using a ZAF program. The analytical conditions were as follows: current intensity 4 nA; accelerating voltage 15 kV; spot size 2 to 4 μm; counting time 10 s per element. The total error on the analyzed elements is <1.5%.

The XRD studies were carried out using a Siemens Kristalloflex 810 diffractometer (40 kV, 30 mA) and Ni-filtered $CuK\alpha_{1,2}$ radiation ($d$ = 1.5406 Å). Samples were examined as random powders and Ca-saturated parallel-oriented clay mineral aggregates. Additional treatments of the specimens included K or Li saturation and solvation with ethylene glycol. The XRD patterns were obtained using a DACO-MP multichannel recorder associated with a microcomputer using the Diffract AT software (SOCABIM). The XRD patterns were decomposed into their elementary component curves using an X-ray decomposition program (DECOMPXR, Lanson, 1993). Such decomposition is assumed to improve the measurement of the positions and relative intensities of the diffraction peaks.

The Hofmann and Klemen (1950) procedure, which involves neutralization of the octahedral negative charge in dioctahedral smectites by Li saturation and heating at 300ºC, was used to determine the location of the layer charge. The Harward *et al*. (1969) procedure which is K saturation and heating at 110ºC was used to differentiate smectite (low charge) from vermiculite (high charge). The smectite mean layer charge was calculated using the method of Olis *et al*. (1990) who proposed an empirical method to determine the mean layer charge from $d_{001}$ values obtained after expansion of the clay minerals with single, long chain alkylammonium ions ($n$C = 12).

Infrared spectra were recorded over the range 4000–400 $cm^{-1}$ on a Nicolet 510 FTIR spectrometer using pressed disks containing an homogeneous mixture of 1 mg of clay and 150 mg of KBr. The spectrometer was continuously purged with dry air during the scanning of the transmission spectra. These disks were placed in a drying oven at 110ºC for 12 h before IR analysis.

Differential thermal analysis (DTA) curves were acquired between 20 and 1100ºC at a rate of 10ºC/min on 15 mg of clay sample with a NETZSCH 409 EP thermal analyzer.

$^{57}Fe$ Mössbauer absorption spectra over the range ±14 mm/s in 512 channels were recorded in the 'Laboratoire de Chimie de Coordination' (Toulouse, France). The Mössbauer spectrometer is composed of a

https://doi.org/10.1346/CCMN.2004.05206013 Published online by Cambridge University Press

compact detector γ system for high counting rates and a 'Wissel' conventional constant acceleration Mössbauer device. A $^{57}$Co (in Rh) source with nominal activity of 50 mCi was used. The spectra were obtained at 80 K to benefit the 2$^{nd}$ order Doppler effect and recorded on a Cambera multichannel analyzer, coupled to a computer. The isomer shift was recorded with respect to α-Fe metal. On the basis of the results of Rancourt *et al.* (1993), the absorber sample thickness was approximated to values for phyllosilicates of the phlogopite–annite series. The values are ~200 mg/cm$^2$ of mineral. Powders were finely ground under acetone (to minimize possible oxidation of Fe) and placed in the plexiglass sample holder. Lorentzian line shapes were assumed for deconvolutions, based on least squares fitting procedures. The $\chi^2$ and misfit values were used to measure the goodness of fit. For phyllosilicate minerals (Rancourt *et al.*, 1992, 1993; Rancourt, 1994a, 1994b), no orientation effects are observed: the electric field gradients of [6] $Fe^{3+}$, [4] $Fe^{3+}$ and [6] $Fe^{2+}$ have different orientations.

## RESULTS

### *Unweathered rock*

The rock is a schistose serpentinite. Under polarized light, the serpentine minerals present different morphologies: (1) pseudomorphic textures formed from olivine (mesh and hourglass structures) or from pyroxene and amphibole (thin blades); (2) serpentine fiber rims around mesh and hourglass structures; and (3) cross-cutting serpentine lodes (chrysotile). Some magnetites and chromites surrounding the mesh or hourglass textural units are included in serpentine fiber rims. The magnesian chlorite appears as a characteristic green, well crystallized mineral (100 μm), intimately associated with serpentine. Some tremolite may occur in the unweathered rock as a serpentinization effect and can be distinguished from the transported tremolite in the allochthonous deposit. Such heterogeneity of the rock may be observed only locally.

The chemical analysis of the unweathered rock is given in Table 1. It is mainly composed of serpentine with minor chlorite and magnetite, consequently the rock chemistry is characterized by high Mg and Si contents. The Mg chlorite is the only Al-bearing mineral in the rock. As a consequence, the Al behavior in the profile will be governed directly by the chlorite weathering processes. The Fe content is related to the magnetite and chromite.

The XRD pattern of the unweathered rock is illustrated in Figure 2. The 7.30, 4.56, 3.65, 2.65 and 2.49 Å reflections are characteristic of serpentine minerals: lizardite and chrysotile. Chlorite gives a regular series of basal spacings at 14.20, 7.10, 4.74, 3.56 and 2.85 Å which did not change after ethylene glycol saturation. The 060 and 062 reflections at 1.54 and 1.50 Å revealed the trioctahedral character of the chlorite and the presence of a type IIb structural unit respectively (Shirozu, 1978; Bailey, 1980).

### *Weathered horizons*

The mineralogical transformations of the serpentinite during the weathering processes were estimated by the relative intensities of XRD reflections for each primary and accessory mineral (Table 2). The chlorite minerals are preserved in the upper horizons and are more stable than serpentines, especially in the advanced weathering stage. The clay minerals appear early in the saprock horizon, due to the early serpentine weathering. The XRD patterns of magnetic particles show that rock magnetite is locally transformed into goethite and to a lesser extent into hematite.

The description and the properties of the weathering profile are given in Table 3. The Munsell soil color

Table 1. Chemical composition (wt.%) of the rock and the weathering samples from ICP-AES analyses.

| Depth (cm) | $SiO_2$ | $Al_2O_3$ | $Fe_2O_3$ | MnO | MgO | CaO | $Na_2O$ | $K_2O$ | $TiO_2$ | $P_2O_5$ | LOI** | Total |
|---|---|---|---|---|---|---|---|---|---|---|---|---|
| Deposit 50–65 | 36.33 | 8.36 | 29.38 | 0.88 | 8.06 | 0.68 | 0.29 | 0.60 | 0.38 | 0.09 | 14.16 | 99.21 |
| Upper saprolite 65–80 | 32.69 | 7.32 | 25.59 | 0.76 | 16.01 | 0.26 | 0.07 | 0.19 | 0.16 | 0.09 | 16.04 | 99.18 |
| Lower saprolite 80–100 | 33.80 | 6.26 | 24.36 | 0.59 | 14.92 | <D.L. | <D.L. | 0.06 | 0.09 | 0.06 | 19.32 | 99.46 |
| Upper saprock 100–120 | 39.29 | 5.44 | 18.34 | 0.25 | 15.93 | 1.09 | <D.L. | 0.05 | 0.17 | 0.08 | 19.09 | 99.73 |
| Lower saprock 120–140 | 37.97 | 4.01 | 18.81 | 0.06 | 19.10 | 0.12 | <D.L. | <D.L. | 0.06 | 0.07 | 20.09 | 100.29 |
| Rock 140 | 39.61 | 1.49 | 7.79* | 0.08 | 36.41 | <D.L. | <D.L. | <D.L. | <D.L. | 0.08 | 14.60 | 100.06 |

D.L.: detection limit
*Total Fe as FeO
** LOI: loss on ignition

https://doi.org/10.1346/CCMN.2004.05206013 Published online by Cambridge University Press

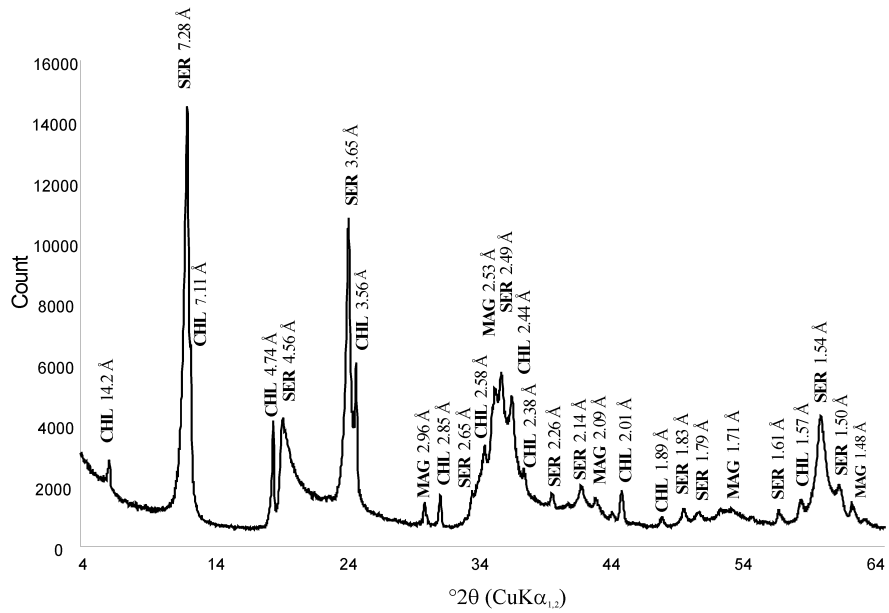


Figure 2. XRD powder pattern of the unweathered rock sample. CHL: chlorite; SER: serpentine; MAG: magnetite.

typifies a brown soil profile; the pH is neutral and the particle-size distribution is dominated by the clay particles (40%). Because of the clay abundance, high total CEC values were measured with dominant exchangeable Mg.

The chemical analyses of each horizon are given in Table 1. The relative element variation is given in Figure 3. For example, the log Mg value is close to −0.3 down to 70 cm depth. Then, the ratio between weathered element and rock element reaches [inv log (−0.3)] = 0.5. This value means that Mg is half as abundant in weathered material as in rock. The elements show three different behaviors: (1) the early leaching of Mg; (2) the stability of Si; and (3) the relative enrichment of Fe and Al to up three to four times rock concentration. Calcium, $Na^+$, $K^+$ and $Ti^{4+}$ cations, which are virtually absent in the rock, are present in measurable abundances in weathered horizons, especially towards the surface, and are assumed to result from an allochthonous contamination. These element contents are partly due to tremolite and K-feldspar occurrence in soil. Local Ca and Ti enrichment due to the heterogeneity of the rock occurs at 110 cm depth, corresponding to the presence of tremolite and titanomagnetite.

Composition-volume diagrams (Figure 4) show the mass oxide variation according to different volume factor values. As observed above, Mg is strongly leached throughout the profile, and Si has a similar behavior, in contrast to its stability recorded in the relative variation calculation above. The discrepancy in Si behavior between calculation methods is relevant to the consideration of volume and mass in composition-volume diagrams. Iron and Al tend to increase in weathered horizons, especially towards the surface.

The results for the different forms of Fe, Al and Si and their proportions in each horizon are given in Table 4. We notice that almost the entire Si and Al content in all fractions belongs to the structure of silicates whereas Fe is distributed variously into silicates and oxyhydroxides depending on depth. The silicate Fe

Table 2. Mineralogical evolutions estimated by the relative intensities of XRD reflections for whole-rock and weathering samples.

| | Depth (cm) | Serpentine | Chlorite | Magnetite chromite | Quartz | Tremolite | Clay minerals | Secondary oxyhydroxides |
|---|---|---|---|---|---|---|---|---|
| Deposit | 50−65 | * | *** | | *** | | ** | *** |
| Upper saprolite | 65−80 | | **** | | ** | | ** | ** |
| Lower saprolite | 80−100 | * | *** | | * | | **** | *** |
| Upper saprock | 100−120 | * | *** | | | ** | *** | * |
| Lower saprock | 120−140 | ** | *** | * | | | *** | |
| Rock | 140 | **** | **** | *** | | | | |

**** predominant; *** dominant: ** abundant; * minor

https://doi.org/10.1346/CCMN.2004.05206013 Published online by Cambridge University Press

Table 3. Pedological description and properties of the different horizons observed in the weathering profile.

| | Depth (cm) | Density ($g/cm^3$) | Munsell soil color | pH $H_2O$ | Carbon content (g/kg) | Organic matter (g/kg) | Particle-size distribution (%) Clay | Fine silt | Coarse silt | Fine sand | Coarse sand |
|---|---|---|---|---|---|---|---|---|---|---|---|
| Saprolite | 65–80 | 1.5 | 10YR 4/4 | 6.9 | 6.9 | 11.9 | 40.9 | 27.9 | 11.4 | 6.5 | 13.2 |
| | 80–100 | 1.5 | 10YR 4/4 | 6.8 | 5.4 | 9.3 | 38.8 | 27.4 | 7.2 | 11.4 | 15.2 |
| Saprock | 100–120 | 1.5 | 10YR 5/6 | 6.8 | 3.3 | 5.7 | 39.6 | 27.9 | 19.4 | 6.3 | 6.7 |
| | 120–140 | 1.2 | 10YR 5/6 | 6.8 | 2.6 | 4.5 | 41.8 | 29.8 | 20.8 | 0.4 | 7.3 |
| Rock | 140 | 2.2 | | | | | | | | | |

| | CEC (cmol(+)/kg) | Exchangeable bases Mg | Ca | Na | K | Saturation (%*) |
|---|---|---|---|---|---|---|
| Saprolite | 28.5 | 11.04 | 0.18 | 0.13 | 0.11 | 40.2 |
| | 39.8 | 14.60 | 0.28 | 0.18 | 0.14 | 38.2 |
| Saprock | 40.9 | 17.60 | 0.27 | 0.16 | 0.13 | 44.4 |
| | 38.7 | 15.30 | 0.30 | 0.15 | 0.08 | 40.9 |

*Saturation %: (Σ exchangeable bases)/(CEC) (%)

shows a decreasing trend towards the surface, with percentages ranging from 75 to 50%, reflecting the increase in oxyhydroxide Fe. The oxy-hydroxide Fe consists of 89% of crystalline Fe.

*Bulk clay mineralogy*

The XRD patterns of random powders show a similar clay mineralogy in all separated fractions, the only variation being the amount of residual primary minerals. The <0.05 μm clay fraction, with a very small primary mineral content was chosen for further XRD and chemical study for each horizon. The XRD patterns of oriented Ca-saturated aggregates (<0.05 μm), air dried and ethylene glycol solvated (Figure 5a), display smectite characteristics. The $d_{001}$ value at 17.20 Å on K-saturated, 110ºC-heated, and ethylene glycol-solvated specimens indicates that it is a low-charged smectite (Harward *et al*., 1969). Intercalation of alkylammonium ions ($n$C = 12) leads to a $d_{001}$ value of 16.70 Å indicating a mean layer charge of 0.34 per half unit-cell (Figure 5b). The position of the $d_{06-33}$ peaks at 1.51 Å indicates an Fe-bearing dioctahedral smectite. The decomposition of the $d_{06-33}$ peak was performed to determine the main contributions of individual components in the fine clay fraction. The decomposition shows the main component at 1.51 Å and two weak components at 1.49 Å and at 1.53 Å which may be attributed to a serpentine mineral or an aluminous dioctahedral smectite and a trioctahedral smectite (saponite), respectively (Figure 5c).

The XRD pattern of the Li-saturated and ethylene-glycol solvated specimens (<0.05 μm) is typical of an expanded smectite with rational series of 17.20 and 8.60 Å reflections. This Li-smectite, after heating at 300ºC and ethylene glycol solvation, appears to be composed of two layer populations: (1) collapsed montmorillonite layers with little or no tetrahedral charge producing a reflection at 9.60 Å; and (2) expanded layers with tetrahedral charge producing a 17.20 Å reflection. The lack of a 002 reflection at 8.60 Å in a Li-300ºC-EG XRD pattern may result from: (1) the small amount of expanded layers; or (2) interstratification of collapsed and expanded layers with non-rational reflection series (Figure 5d).

The DTA curves of the fine clay fraction show a dehydroxylation endothermic peak beginning at 350–400ºC, up to 550ºC. The greatest loss of hydroxyl water occurs at lower temperatures for nontronite (<550ºC) than it does for beidellite (600ºC) and montmorillonite (700ºC). Thus, the endothermic peak on the

Table 4. Percentages of elements Si, Al and Fe in different forms (silicate or oxide) in the profile. (1) Crystalline Fe oxide: [($Fe_d$–$Fe_o$)/Total Fe]; (2) poorly crystalline Fe oxide: [$Fe_o$/Total Fe].

| Depth (cm) | Fe (%) Silicate Fe | Crystalline oxide Fe(1) | Poorly crystalline oxide Fe(2) | Si (%) Silicate Si | Amorphous Si | Al (%) Silicate Al | Amorphous Al |
|---|---|---|---|---|---|---|---|
| 50–65 | 51.10 | 43.58 | 5.31 | 99.34 | 0.66 | 96.01 | 3.99 |
| 65–80 | 47.00 | 45.94 | 7.06 | 98.95 | 1.05 | 99.19 | 0.81 |
| 80–100 | 55.16 | 37.71 | 7.13 | 98.45 | 1.55 | 99.82 | 0.18 |
| 100–120 | 71.67 | 22.22 | 6.10 | 98.27 | 1.73 | 100.00 | 0.00 |
| 120–140 | 75.06 | 17.34 | 7.60 | 97.68 | 2.32 | 100.00 | 0.00 |

https://doi.org/10.1346/CCMN.2004.05206013 Published online by Cambridge University Press

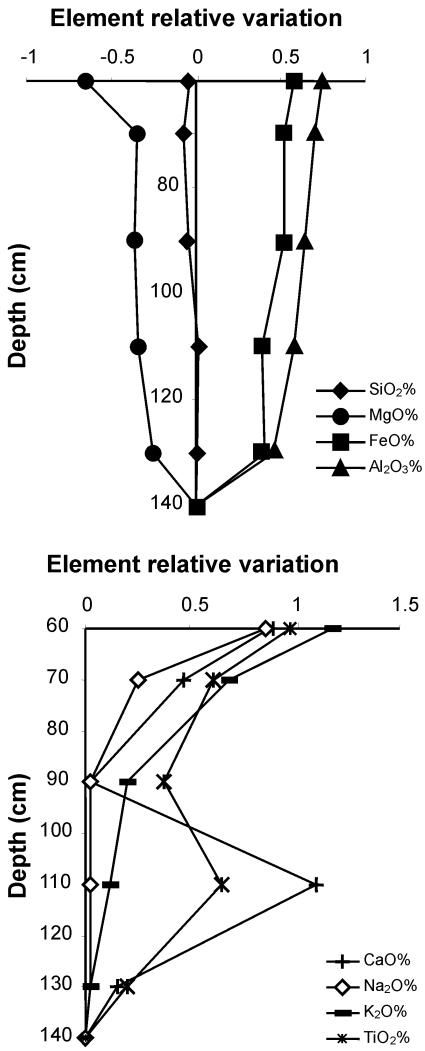


Figure 3. Relative variations of major elements according to depth.

curve is characteristic of nontronite, the presence of much Fe depressing the temperature of the endothermic dehydroxylation peak below 550ºC (Mackenzie, 1970).

Table 5 lists calculated parameters from Mössbauer spectra of the <0.05 μm clay samples. In three specimens located near the surface, some Fe oxide was detected and is probably goethite, in agreement with XRD patterns. Deconvolution of the resulting spectra permits the quantification of the proportions of these oxides; the values are 18%, 38% and 30% from the bottom to the top of the profile. The higher values correspond to the saprolite clays whereas the lower is located at the top of the saprock horizon. In all samples, the Fe in silicate minerals is $Fe^{3+}$ in octahedral sites. No trace of ferrous Fe was detected, even in the deepest sample.

The chemical analyses (% oxides) using electron microprobe (WDS) are performed on pressed Ca-saturated fine-clay fraction (<0.05 μm) pellets of

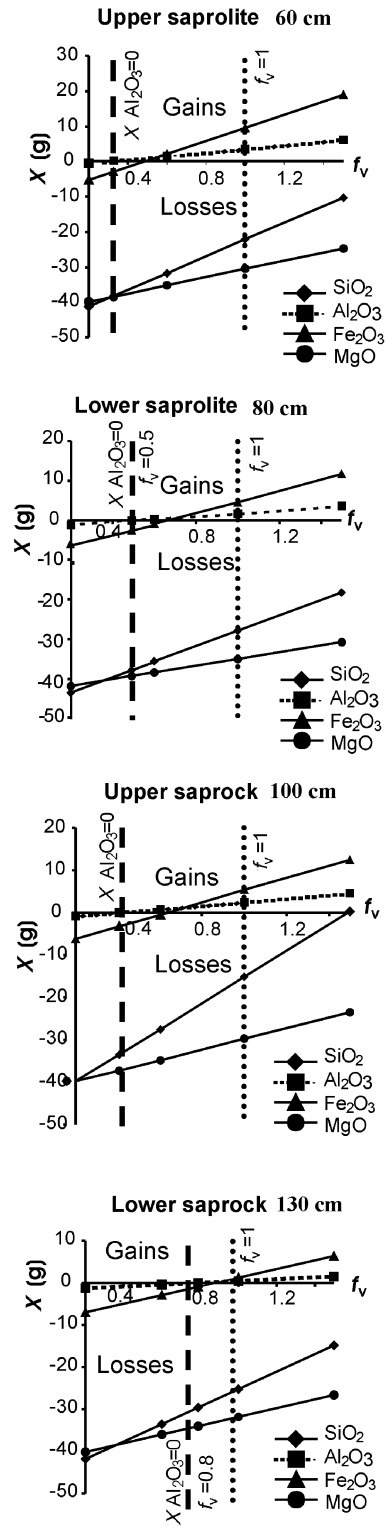


Figure 4. Composition-volume diagrams according to depth. Gains (positive values) and losses (negative values) of major elements during weathering assuming either: (1) $f_v$ = 1: isovolumetric condition (saprock horizon); or (2) $X\ Al_2O_3 = 0$: immobile Al condition (saprolite horizon).

https://doi.org/10.1346/CCMN.2004.05206013 Published online by Cambridge University Press

Table 5. Parameters from Mössbauer spectra recorded at 80 K.

| | Depth (cm) | Silicate QS | Silicate IS | Silicate % | Oxide QS | Oxide IS | Oxide H(T)% | Oxide % |
|---|---|---|---|---|---|---|---|---|
| Deposit | 50–65 | 0.367 | 0.444 | 70 | 0.005 | 0.445 | 47.523 | 30 |
| Upper saprolite | 65–80 | 0.331 | 0.449 | 62 | −0.246 | 0.454 | 47.129 | 38 |
| Lower saprolite | 80–100 | 0.304 | 0.424 | 100 | | | | 0 |
| Upper saprock | 100–120 | 0.328 | 0.453 | 82 | −0.264 | 0.496 | 47.224 | 18 |
| Lower saprock | 120–140 | 0.316 | 0.453 | 100 | | | | 0 |
| Rock | 140 | 0.333 | 0.445 | 100 | | | | 0 |

QS: quadrupole splitting
IS: isomer shift relative to α-Fe metal
H(T)%: magnetic field in Tesla
%: percentages of silicates and oxides

saprock and saprolite horizons previously studied by XRD (see Figure 5a–d). The Mössbauer data indicate that the majority of iron (70%) was located in clay structures under $Fe^{3+}$ oxidation state in octahedral sites. Pellet chemical analyses were then corrected from 30% Fe located in oxide structure. For previous XRD data (especially Figure 5a,d) showing only smectite occurrence, the chemical analyses were used to calculate a mean structural formulae on the basis of 11 oxygen atoms (Table 6). The result shows that the <0.05 μm clay fraction has a smectite composition mainly characterized by a dioctahedral occupancy. Iron is the

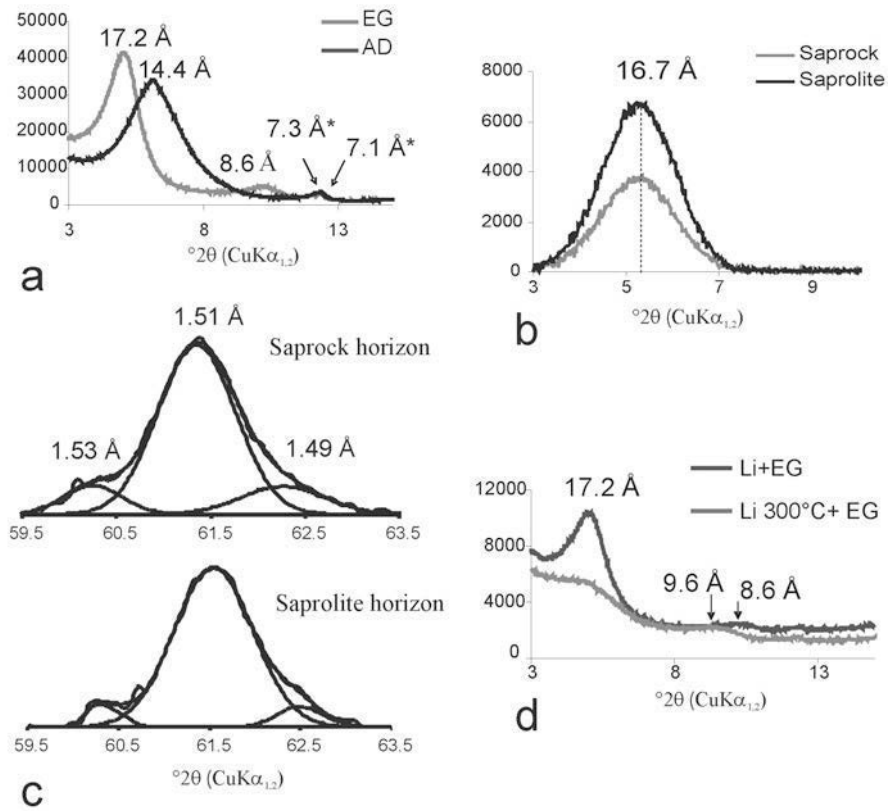


Figure 5. (a) Oriented XRD patterns of Ca-saturated smectite (<0.05 μm), air dried (AD) and ethylene glycol solvated (EG). *7.3 Å: 001 serpentine. *7.1 Å: 002 chlorite. (b) Oriented XRD patterns of alkylammonium-saturated smectite (<0.05 μm). Method of Olis *et al*. (1990): empirical method to determine the mean layer charge (MLC) from $d_{001}$ values obtained after expansion of the clay minerals with single, long-chain alkylammonium ions ($n$C = 12). $d_{001}$ = 16.7 Å; $d_{001}$ = 5.52 + 32.98 MLC; MLC = 0.34 per half unit-cell (Olis *et al*., 1990). (c) Decomposition of the $d_{06.33}$ peak of Ca-saturated smectite (<0.05 μm) for saprock and saprolite horizons. (d) XRD patterns of oriented Li-saturated smectite (<0.05 μm), ethylene glycol solvated before heating (Li + EG) and after heating at 300ºC (Li300ºC + EG): determination of the layer charge location by the Hofmann and Klemen (1950) procedure.

https://doi.org/10.1346/CCMN.2004.05206013 Published online by Cambridge University Press

prevailing octahedral cation. Some chemical variations, from saprock to saprolite, are observed: (1) the Al content increases significantly (0.53 to 0.97 atoms); (2) the Fe content decreases (1.47 to 1.10 atoms); (3) the Mg content seems to be almost constant (0.25–0.37 atoms); and (4) the total charge decreases slightly (0.61 to 0.37), balanced by a decrease in the Ca content in relation to decreasing interlayer charge.

The Hofmann and Klemen treatment has revealed two smectite layer populations in both saprock and saprolite clays (<0.05 μm): montmorillonite and nontronite types. These two populations are also distinguished using electron microprobe data. The chemical analyses of these phases are scattered along a mixing line between two poles: (1) a smectite with small tetrahedral charge, *i.e.* montmorillonite; and (2) a smectite with large tetrahedral charge. Considering that Fe is the prevalent octahedral cation, these smectites can be identified as Fe montmorillonite and nontronite. This chemical trend is better shown in the saprolite than in the saprock where the composition range is more restricted in the 0.25–0.36 tetrahedral Al range. This could be related to an insufficient number of analyses. However, the composition ranges of clays in saprock and saprolite are clearly separated on the basis of both total Fe and Al contents (Figure 7a).

Table 6. Structural formula per half unit-cell (11 oxygens) of the Ca-saturated smectites (<0.05 μm) calculated from electron microprobe analyses (WDS).

| Saprock: 100–140 cm (17 analyses) | | | | | | | | | |
|---|---|---|---|---|---|---|---|---|---|
| Si | $^{IV}$Al | $^{VI}$Al | Octahedral occupancy | Charge (VI) | Total charge | Interlayer charge (exchangeable Ca) | Al total | $Fe^{3+}$ | Mg |
| 3.69 | 0.31 | 0.25 | 2.09 | 0.13 | 0.45 | 0.41 | 0.56 | 1.41 | 0.34 |
| 3.64 | 0.36 | 0.22 | 2.12 | 0.06 | 0.42 | 0.38 | 0.58 | 1.45 | 0.35 |
| 3.64 | 0.36 | 0.20 | 2.04 | 0.25 | 0.61 | 0.55 | 0.56 | 1.43 | 0.32 |
| 3.68 | 0.32 | 0.24 | 2.07 | 0.18 | 0.50 | 0.43 | 0.56 | 1.41 | 0.32 |
| 3.69 | 0.31 | 0.24 | 2.07 | 0.18 | 0.49 | 0.44 | 0.56 | 1.41 | 0.31 |
| 3.69 | 0.31 | 0.25 | 2.08 | 0.16 | 0.46 | 0.42 | 0.56 | 1.41 | 0.32 |
| 3.71 | 0.29 | 0.27 | 2.07 | 0.17 | 0.46 | 0.41 | 0.56 | 1.38 | 0.32 |
| 3.75 | 0.25 | 0.28 | 2.02 | 0.27 | 0.52 | 0.42 | 0.54 | 1.37 | 0.28 |
| 3.68 | 0.32 | 0.25 | 2.07 | 0.16 | 0.48 | 0.43 | 0.57 | 1.43 | 0.31 |
| 3.71 | 0.29 | 0.28 | 2.05 | 0.22 | 0.51 | 0.47 | 0.57 | 1.38 | 0.30 |
| 3.71 | 0.29 | 0.28 | 2.06 | 0.19 | 0.48 | 0.43 | 0.57 | 1.38 | 0.32 |
| 3.67 | 0.33 | 0.25 | 2.08 | 0.13 | 0.46 | 0.44 | 0.58 | 1.43 | 0.32 |
| 3.72 | 0.28 | 0.25 | 2.06 | 0.17 | 0.45 | 0.42 | 0.53 | 1.42 | 0.30 |
| 3.69 | 0.31 | 0.23 | 2.06 | 0.16 | 0.47 | 0.43 | 0.53 | 1.45 | 0.30 |
| 3.67 | 0.33 | 0.25 | 2.09 | 0.12 | 0.45 | 0.41 | 0.57 | 1.43 | 0.32 |
| 3.65 | 0.35 | 0.20 | 2.06 | 0.18 | 0.53 | 0.48 | 0.55 | 1.47 | 0.31 |
| 3.73 | 0.27 | 0.27 | 2.06 | 0.18 | 0.46 | 0.42 | 0.54 | 1.41 | 0.30 |

| Saprolite: 65–100 cm (19 analyses) | | | | | | | | | |
|---|---|---|---|---|---|---|---|---|---|
| Si | $^{IV}$Al | $^{VI}$Al | Octahedral | Charge (VI) occupancy | Total charge | Interlayer charge (exchangeable Ca) | Al total | $Fe^{3+}$ | Mg |
| 3.64 | 0.36 | 0.51 | 2.12 | 0.05 | 0.41 | 0.36 | 0.87 | 1.17 | 0.36 |
| 3.65 | 0.35 | 0.56 | 2.13 | 0.04 | 0.40 | 0.37 | 0.91 | 1.12 | 0.37 |
| 3.64 | 0.36 | 0.52 | 2.12 | 0.05 | 0.41 | 0.36 | 0.88 | 1.18 | 0.34 |
| 3.69 | 0.31 | 0.59 | 2.10 | 0.06 | 0.37 | 0.34 | 0.90 | 1.13 | 0.30 |
| 3.65 | 0.35 | 0.55 | 2.11 | 0.04 | 0.39 | 0.36 | 0.90 | 1.17 | 0.32 |
| 3.80 | 0.20 | 0.52 | 2.03 | 0.22 | 0.42 | 0.38 | 0.72 | 1.18 | 0.25 |
| 3.80 | 0.20 | 0.54 | 2.03 | 0.24 | 0.43 | 0.39 | 0.73 | 1.15 | 0.27 |
| 3.72 | 0.28 | 0.51 | 2.08 | 0.11 | 0.39 | 0.36 | 0.79 | 1.20 | 0.28 |
| 3.82 | 0.18 | 0.54 | 2.03 | 0.22 | 0.40 | 0.37 | 0.73 | 1.16 | 0.25 |
| 3.76 | 0.24 | 0.52 | 2.04 | 0.20 | 0.44 | 0.41 | 0.76 | 1.19 | 0.26 |
| 3.64 | 0.36 | 0.53 | 2.12 | 0.03 | 0.39 | 0.36 | 0.89 | 1.17 | 0.34 |
| 3.64 | 0.36 | 0.57 | 2.13 | 0.00 | 0.36 | 0.34 | 0.93 | 1.15 | 0.33 |
| 3.81 | 0.19 | 0.54 | 2.02 | 0.25 | 0.44 | 0.39 | 0.73 | 1.14 | 0.26 |
| 3.79 | 0.21 | 0.58 | 2.05 | 0.18 | 0.38 | 0.35 | 0.79 | 1.12 | 0.27 |
| 3.76 | 0.24 | 0.59 | 2.06 | 0.15 | 0.38 | 0.35 | 0.82 | 1.12 | 0.30 |
| 3.80 | 0.20 | 0.60 | 2.04 | 0.19 | 0.39 | 0.36 | 0.80 | 1.10 | 0.27 |
| 3.69 | 0.31 | 0.52 | 2.04 | 0.21 | 0.52 | 0.47 | 0.83 | 1.16 | 0.29 |
| 3.54 | 0.46 | 0.49 | 2.15 | −0.01 | 0.44 | 0.39 | 0.95 | 1.20 | 0.37 |
| 3.53 | 0.47 | 0.49 | 2.16 | −0.08 | 0.40 | 0.36 | 0.97 | 1.23 | 0.36 |

https://doi.org/10.1346/CCMN.2004.05206013 Published online by Cambridge University Press

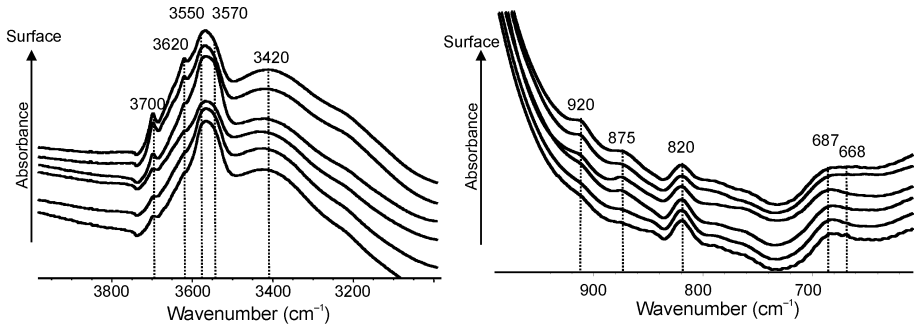


Figure 6. (a) FTIR spectra according to depth of Ca-saturated smectite (<0.05 μm) in the νOH region. (b) FTIR spectra according to depth of Ca-saturated smectite (<0.05 μm) in the δOH region.

The IR spectrum of a fine clay fraction from saprock and saprolite is similar to a nontronite spectrum. In the OH-stretching region (Figure 6a), a broad absorption band between 3550 and 3580 cm$^{-1}$ was attributed to several contributions of individual structural OH groups probably occurring in the octahedral sheet of the fine clay fraction, indicating an Fe-rich smectite. The main components at 3550 and 3570 cm$^{-1}$ were attributed to $\nu Fe_2^{3+}OH$ and $\nu Fe^{3+}AlOH$, respectively (Farmer, 1974; Goodman *et al*., 1976; Madejová *et al*., 1994; Petit *et al*., 2002). That there were no trioctahedral occupancies was indicated by a band at 3680 cm$^{-1}$ ($\nu Mg_3OH$). Weak absorption bands at 3690 and 3620 cm$^{-1}$ with increasing intensities in the upper part of the soil profile were attributed to $\nu_1 Al_2^{3+}OH$ and $\nu_4 Al_2^{3+}OH$, respectively, and are characteristics of a kaolinite spectrum. However, XRD did not detect kaolinite in the fine clay fraction. The IR spectra may indicate a small kaolinite content especially towards the surface in the interface with the allochthonous deposit. Kaolinite is commonly present in smectite-rich samples though it is not detected by XRD (Delvaux *et al*., 1989; Petit *et al*., 1992; Madejová *et al*., 1995). Kaolinite can be detected in amounts from 7‰ and be characterized in smectite-rich samples by an absorption band at 3690 cm$^{-1}$ for abundances >1% (Joussein *et al*., 2001).

In the OH-bending region (Figure 6b), there were two main absorption bands at 874 and 819 cm$^{-1}$ which were assigned to $\delta AlFe^{3+}OH$ (Farmer, 1974) and $\delta Fe_2^{3+}OH$ (Goodman *et al*., 1976), respectively. The absorption band at 874 cm$^{-1}$ tends to increase in intensity towards the surface whereas that at 819 cm$^{-1}$ decreases slightly. This evolution may be interpreted as the integration of Al in the smectite octahedral sheet in place of Fe. The increase of the band at 920 cm$^{-1}$ ($\delta Al_2^{3+}OH$) (Farmer, 1974) towards the surface was probably due to the kaolinite contribution. However, as no kaolinite was detected by XRD, its amount will be <5% (XRD detection limit) and thus, its contribution to Al contents in the clay minerals can be ignored. In the region between 600 and 750 cm$^{-1}$, there was an absorption band at 685 cm$^{-1}$ attributed to $Si-O-^{VI}Fe$ (Farmer, 1974).

The IR data permit the conclusions that: (1) there was little variation in smectite composition with profile depth: the Al content in the octahedral sheet seems to increase towards the surface whereas the Fe content decreases slightly; (2) in all samples, Fe is the prevailing octahedral cation but Al is also present in the octahedral sheet; (3) there were no discernible absorption bands corresponding to $\delta Fe^{3+}MgOH$ and $\delta Al^{3+}MgOH$, indicating that Mg is not present in the octahedral sheet and there is no evidence of Mg in trioctahedral sites.

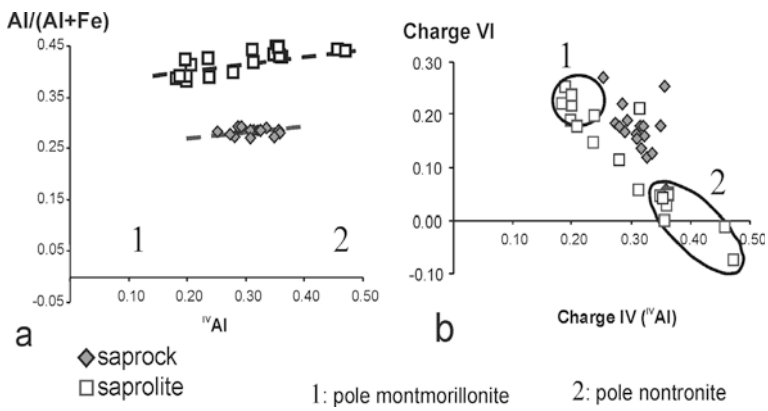


Figure 7. Chemical variation between saprock and saprolite Ca-saturated smectites (<0.05 μm). (a) Relationship between tetrahedral charge and total Al and Fe contents of smectites. (b) Relationship between the tetrahedral and octahedral smectite charges.

https://doi.org/10.1346/CCMN.2004.05206013 Published online by Cambridge University Press

## DISCUSSION

### *Weathering characteristics*

In the early weathering stage where the rock structure is well preserved, petrographic observations show that the serpentine minerals are brown colored which indicates the replacement of the serpentine mineral by clay minerals. The particle-size distribution indicates that clay minerals appear appreciably at the saprock horizon, with the clay percentage reaching 37% below 120 cm depth. Relative intensities of XRD reflections for each primary mineral (Table 2) show that serpentine decreases in abundance early when compared to the chlorite. The chemical analyses of each horizon in comparison with the unweathered rock shows the relative enrichment of the Fe and Al relative to Mg. Bulk mass-balance shows that leaching of both Mg and Si occurred, reflecting the early destabilization of serpentine minerals. Part of this Mg appears as interlayer exchangeable cations (15 cmol(+)/kg), in comparison with Ca, Na and K which are <0.3 cmol(+)/kg. The IR data show (1) no evidence for trioctahedral occupancy and (2) no discernible Mg presence in the structure. All arguments demonstrate that the dominant rock alteration processes are (1) the early serpentine weathering inducing important leaching of Mg and (2) the relative immobility of Al and Fe in the profile (relative stability of chlorite and magnetite in comparison with serpentine minerals), both elements which will control the clay mineral formation during weathering. Indeed, bulk clay mineralogy indicates an Al- and Fe-rich smectite composition.

### *Evolution of bulk-clay chemistry*

Chemical analyses, using electron microprobe, of the clay fraction indicate an Al content increasing towards the surface, as supported by IR data which show increasing octahedral Al content in clays from upper horizons.

This bulk-clay evolution is due to the chemical weathering of the only Al-bearing mineral in the rock, *i.e.* chlorite. This weathering mineral liberates increasing amounts of Al to the upper horizons, which is partially trapped in Fe-rich smectites and in kaolinite near the interface with the allochthonous deposit. Iron, which increases in the bulk samples (see Table 1) but decreases from saprock to saprolite clays (<0.05 μm) is mobilized to form oxides.

### *Charge variation*

The smectite mean layer charge calculated in accordance with the method of Olis *et al*. (1990) varies between the values of 0.33 and 0.36 per half unit-cell in the profile and characterizes a low-charge smectite. However, the structural formulae on the basis of 11 oxygen atoms calculated from chemical analyses of the clay fraction using electron microprobe (Table 6) shows that the total charge decreases slightly from saprock to saprolite. In agreement with total charge decrease, the Ca content in the interlayer of Ca-saturated clay fraction decreases.

The relationship between the tetrahedral and octahedral smectite charges is given in Figure 7b. The tetrahedral charge resulting entirely from Si-Al substitutions (sufficient Al to balance the Si deficit) is well correlated with the octahedral charge calculated with excess Al, total Fe and Mg. Two poles can be distinguished in saprock and saprolite clays: one pole with high tetrahedral charge and no octahedral charge is of nontronite-beidellite type, and another pole with octahedral charge and low tetrahedral charge is of Fe-rich montmorillonite type. A more detailed relationship between tetrahedral charge and total Al and Fe contents (Figure 7a) indicates that a discrimination exists between saprock and saprolite clays. Considering the tetrahedral charges, the clay minerals in saprock and saprolite exhibit the same chemical trend between low and high tetrahedral charges. However, considering total Al and Fe contents, these clays differentiate into two chemical composition domains, Fe-rich for saprock clays and Al-rich for saprolite clays.

These observations indicate that the general weathering in this profile is to form Fe and Al clay minerals, in good agreement with (1) the leaching of Mg out of the profile and (2) the relative immobility of Al and Fe. The chemical discrepancy between saprock and saprolite clays (Fe *vs*. Al compositions) could be related to the formation of oxides in the saprolite. These oxides could have trapped most of the Fe available in the saprolite horizons, creating an Fe-depleted environment for clay mineral crystallization.

## CONCLUSIONS

This work demonstrates that, even in Mg-rich weathering systems, ferric and aluminous smectites may form due to Mg leaching in the early weathering stages. Moreover, the smectites which crystallize in this system are complex and heterogeneous with regard to the amount of layer charge, the distribution of this larger charge in tetrahedral and/or octahedral sheets, and their chemistry.

Additional results seem to indicate that such mineralogical complexity may arise from the heterogeneity of the weathering microsites in the weathering profile. Actually, weathering of each primary mineral generates particular microsystems with specific morphological, mineralogical and chemical characteristics. As a consequence, we need to identify these microsystems in weathering sequences of each primary mineral in order to improve our understanding of the relationship between bulk clay mineralogy and individual primary mineral contribution and of the weathering processes of serpentinite. These objectives will be the topic of further work.

https://doi.org/10.1346/CCMN.2004.05206013 Published online by Cambridge University Press

## REFERENCES


Alexander, E.B. (1988) Morphology, fertility and classification of productive soils on serpentinised peridotite in California, U.S.A. *Geoderma*, **41**, 337–351.

Alexander, E.B., Adamson, C., Zinke, P.J. and Graham, R.C. (1989) Soils and conifer productivity on serpentinized peridotite of the Trinity ophiolite, California. *Soil Science*, **148**, 412–423.

Bailey, S.W. (1980) Structures of layer silicates. Pp. 1–123 in: *Crystal Structures of Clay Minerals and their X-ray Identification* (G.W. Brindley and G. Brown, editors). Monograph **5**, Mineralogical Society, London.

Berre, A., Ducloux, J. and Dupuis, J., (1974) Pédogénèse sur roches ultrabasiques en climat tempéré humide : les sols sur serpentinites du Limousin occidental. *Extrait de Science du sol – Bulletin de l'A.F.E.S.*, **3**, 135–146.

Besset, F. (1978) Localisations et répartitions successives du nickel au cours de l'altération latéritiques des péridotites de Nouvelle-Calédonie. PhD thesis, France, 129 pp.

Bonifacio, E., Zanini, E., Boero, V. and Franchini-Angela, M. (1996) Pedogenesis in a soil catena on serpentinite in northwestern Italy. *Geoderma*, **75**, 33–51.

Bulmer, C.E and Lavkulich, L.M. (1994) Pedogenic and geochemical processes of ultramafic soils along a climatic gradient in southwestern British Columbia. *Canadian Journal of Soil Science*, **74**, 165–177.

Cleaves, E.T., Fisher, D.W. and Bricker, O.P. (1974) Chemical weathering of serpentinite in the Eastern Piedmont of Maryland. *Geological Society of America Bulletin*, **85**, 437–444.

Coombe, D.E., Frost, L.C., Le Bas, M. and Watters, W. (1956) The nature and origin of the soils over the Cornish serpentine. *Journal of Ecology*, 605–615.

Delvaux, B., Mestdagh, M.M.,Vielvoye, L. and Herbillon, A.J. (1989) XRD, IR and ESR study of experimental alteration of Al-nontronite into mixed layer kaolinite/smectite. *Clay Minerals*, **24**, 617–630.

Ducloux, J., Meunier, A. and Velde, B. (1976) Smectite, chlorite, and a regular interlayered chlorite-vermiculite in soils developed on a small serpentinite body. Massif Central, France. *Clay Minerals*, **11**, 121–135.

Farmer, V.C. (1974) The Layer Silicates. Pp. 331–365 in: *The Infrared Spectra of Minerals* (V.C. Farmer, editor). Monograph **4**, Mineralogical Society, London.

Gaudin, A. (2002) Cristallochimie des smectites du gisement latéritique nickélifère de Murrin Murrin (Ouest Australie). PhD thesis, Université d'Aix-Marseille III, Aix en Provence, France, 265 pp.

Golighty, J.P. (1981) Nickeliferous laterite deposits. *Economic Geology*, **75**, 710–735.

Goodman, B.A., Russell, J.D., Fraser, A.R. and Woodhams, F.W.D. (1976) A Mössbauer and IR spectroscopic study of the structure of nontronite. *Clays and Clay Minerals*, **24**, 53–59.

Graham, R.C., Diallo, M.M. and Lund, L.J. (1990) Soils and mineral weathering on phyllite colluvium and serpentinite in northwestern California. *Soil Science Society of America Journal*, **54**, 1682–1690.

Gresens, R.L. (1967) Composition-volume relationships of metasomatism. *Chemical Geology*, **2**, 47–65.

Harward, M.E., Castea, D.D. and Sayegh, A.H. (1969) Properties of vermiculites and smectites: expansion and collapse. *Clays and Clay Minerals*, **11**, 437–447.

Hofmann, U. and Klemen, R. (1950) Verlust der Austauschfähigkeit von Lithiuminonen an Bentonit durch Erhitzung. *Zeitschrift für anorganische und allgemeine Chemie*, **262**, 95–99.

Isok, J.D. and Harward, M.E. (1982) Influence of soil moisture on smectite formation in soils derived from serpentinite. *Soil Science Society of America Journal*, **46**, 1106–1108.

Joussein, E., Petit, S. and Decarreau, A. (2001) Une nouvelle méthode de dosage des minéraux argileux en mélange par spectroscopie IR. *Comptes Rendus de l'Académie des Sciences*, **332**, 83–89.

Lanson, B. (1993) *DECOMPXR, X-ray Decomposition Program*. ERM, Poitiers, France.

Mackenzie, R.C. (1970) Simple phyllosilicates based on gibbsite- and brucite-like sheets. Pp. 498–534 in: *Differential Thermal Analysis I* (R.C. Mackenzie, editor). Mineralogical Society, London.

Madejová, J., Kraus, I. and Komadel, P. (1995) Fourier transform infrared spectroscopic characterization of dioctahedral smectites and illites from the main Slovak deposits. *Geologica Carpathica - Series Clays*, **1**, 23–32.

Madejová, J., Komadel, P. and Čičel, B. (1994) Infrared study of octahedral site populations in smectites. *Clay Minerals*, **29**, 319–326.

Mehra, O.P. and Jackson, M.L. (1960) Iron oxides removal from soils and clays by dithionite-citrate systems buffered with sodium bicarbonate. *7th national Conference of Clay Minerals*, 317–327.

N'Kanika Wa Rupiya, P. (1979) Etude géochimique des métaux dans les sols développés sur le massif de serpentines de La Roche-l'Abeille (Haute Vienne, France). PhD thesis, Université d'Orléans, France, 120 pp.

Olis, A.C., Malla, P.B. and Douglas, L.A. (1990) The rapid estimation of the layer charges of 2:1 expanding clays from a single alkylammonium ion expansion. *Clay Minerals*, **25**, 39–50.

Pelletier, B. (1983) Localisation du nickel dans les minerais « garnieritiques » de Nouvelle-Calédonie. PhD thesis, Sciences géologiques, Mémoire **73**, Université de Strasbourg, France.

Petit, S., Prot, T., Decarreau, A., Mosser, C. and Toledo-Groke, M.C. (1992) Crystallochemical study of a population of particles in smectites from a lateritic weathering profile. *Clays and Clay Minerals*, **40**, 436–445.

Petit, S., Caillaud, J., Righi, D., Madejová, J., Elsass, F. and Köster, H.M. (2002) Characterization and crystal chemistry of an Fe-rich montmorillonite from Ölberg, Germany. *Clay Minerals*, **37**, 283–297.

Rabenhorts, M.C., Foss, J.E. and Fanning, D.S. (1982) Genesis of Maryland soils formed from serpentinite. *Soil Science Society of America Journal*, **46**, 607–616.

Rancourt, D.G. (1994a) Mössbauer spectroscopy of minerals. I. Inadequacy of Lorentzian-line doublets in fitting spectra arising from quadrupole splitting distributions. *American Mineralogist*, **21**, 244–249.

Rancourt, D.G (1994b) Mössbauer spectroscopy of mineral. II. Problem of resolving cis and trans octahedral $Fe^{2+}$ sites. *American Mineralogist*, **21**, 250–257.

Rancourt, D.G., Dang, M.Z. and Lalonde, A.E. (1992) Mössbauer spectroscopy of tetrahedral $Fe^{3+}$ in trioctahedral micas. *American Mineralogist*, **77**, 34–43.

Rancourt, D.G., McDonald, A.M., Lalonde, A.E. and Ping, J.Y. (1993) Mössbauer absorber thickness for accurate site populations in Fe-bearing minerals. *American Mineralogist*, **78**, 1–7.

Reesman, A.L., Pickett, E.E. and Keller, W.D. (1969) Aluminous ions in aqueous solutions. *American Journal of Science*, **267**, 99–113.

Schwertmann, U. (1964) Differenzierung der Eisenoxide des Bodens durch Extraktion mit Ammoniumoxalat-Lösung. *Zeitschrift fuer Pflanzenernaehrung, Duengung, Bodenkunde*, **105**(3) 194–201.

Shirozu, H. (1978) Chlorite minerals. Pp. 243–264 in: *Clays and Clay Minerals of Japan* (T. Suyo and S. Shimoda,

editors). Elsevier, Amsterdam.
Smith, B.F.L. and Mitchell, B.D. (1987) Characterization of poorly ordered minerals by selective chemical methods. Pp. 275–294 in: *A Handbook of Determinative Methods in Clay Mineralogy*. (M.J. Wilson, editor). Chapman & Hall, London.
Trescases, J.J. (1969) Premières observations sur l'altération des péridotites de Nouvelle-Calédonie. *Pédologie, Géochimie, Géomorphologie*, *cahier. O.R.S.T.O.M., Série. Géologie, Paris*, **1**, 27–57.
Trescases, J.J. (1975) L'évolution géochimique supergène des roches ultrabasiques en zone tropicale. Formations des gisements nickélifères de Nouvelle-Calédonie. PhD thesis, Université de Poitiers, France, 254 pp.
Trescases, J.J. (1986) Nickeliferous laterites: A review on the contributions of the last ten years. *Geological Survey of India, Memoirs*, **120**, 51–62.
Wesolowski, D.J. (1992) Aluminum speciation and equilibria in aqueous solution: The solubility of gibbsite in the system Na-K-Cl-OH-$Al(OH)_4$ from 0 to 100ºC. *Geochimica et Cosmochimica Acta*, **56**, 1065–1091.
Wildman, W.E., Jackson, M.L. and Whittig, L.D. (1968) Iron-rich montmorillonite formation in soils derived from serpentinite. *Soil Science Society of America Proceedings*, **32**, 787–794.

(*Received 11 September 2003; revised 21 July 2004; Ms. 832*)